This article has been accepted for publication in a future issue of this journal, but has not been fully edited. Content may change prior to final publication. Citation information: DOI 10.1109/JSEN.2020.3023178, IEEE Sensors Journal

New Unobtrusive Tidal Volume Monitoring System using Channel State Information in Wi-Fi Signal: Preliminary Result

Jungyoon Kim, Youngchan Jang, Eunshin Byon, *Member*, *IEEE*, Dawn M. Tilbury, *Fellow*, *IEEE*, Milo Engoren, Satya Krishna Ramachandran and Mi-Sun Kang

***Abstract*— In this paper, we propose a respiration monitoring system based on the channel state information received from a commercial off-the-shelf Wi-Fi device. We develop data processing modules for extracting respiration parameters from the Wi-Fi signal and estimate the relative tidal volume. In order to verify the performance of the proposed monitoring system, we use a human patient simulator and also test one real human subject in various experimental settings. With the human patient simulator, we evaluate the monitoring performance at various tidal volume levels and compare our monitoring results with the simulator settings. In testing with a human subject, we test our approach on different sleep postures and positions, Wi-Fi router's positions, and monitoring environments and compare our performance with the spirometer measurement. The results with both the human patient simulator and real human subject demonstrate the strong and robust estimation performance of the proposed approach in various monitoring conditions, indicating the high promise for non-intrusive respiration monitoring in practice.**

***Index Terms*— vital signs, channel state information, non-intrusive monitoring, remote sensing, respiratory rate**

I. Introduction

RECENTLY ubiquitous health monitoring systems have gained increasing attention. Unobtrusive, non-invasive, and long-term health monitoring systems have practical potential to improve individual's health status or quality of life. Such systems aim to collect health information from patients and detect abnormalities over long-term periods in a variety of environments. Among various health metrics, the tidal volume (VT), which is the main focus of this study, and respiratory rate (RR) can capture a person's basic physiologic functions and provide essential features to help determine the person's physical health condition and detect serious problems before they occur.

In particular, maintaining an appropriate respiration pattern during sleep is an important factor for human health. Abnormal respiration patterns during sleep, e.g., due to apnea, may affect activities of daily life, and can even cause serious illness or death. However, respiratory patterns are hard to measure at home without special devices. In general, people do not want to wear devices while sleeping. Devices attached on their body, e.g., face or chest, can be perceived as uncomfortable or claustrophobic. Moreover, some devices attached around the chest such as wearable sensors restrict postures during sleep. Therefore, an automatic respiration monitoring system with an unobtrusive and non-invasive device is useful and needed for detecting respiratory disorders during sleep. In addition to helping to diagnose a sleep disorder, long-term VT and RR monitoring can also be used to capture significant features of other respiratory disorders and to facilitate treatment of medical conditions, such as pneumothorax, pulmonary edema, and chronic obstructive pulmonary disease [1].

Several techniques have been proposed for long-term VT or RR monitoring using different types of sensors, including camera [2, 3], Doppler radar [4], sound sensors [5], laser [6], infrared imaging sensor [7], high-resolution accelerometers [8, 9], and depth camera [10, 11, 12, 13]. Many of these techniques require direct patient contact. For example, Fekr *et al.* [14] proposed to measure RR and VT with a wearable accelerometer sensor attached to the body. However, such devices cause inconvenience to patients and thus prevent long-term monitoring. Some studies use non-contact devices including microphones and vision-based cameras. Although these devices are less obtrusive, they can invoke privacy concerns [1, 5, 15]. Recently, non-invasive respiration monitoring systems based on radio frequency (RF) devices have drawn attention due to their comfortable sensing environment. The received signal strength (RSS) is the most popular approach among RF technologies. However, the measurements from the RSS devices are sensitive to environment conditions and noises, and

J. Y. Kim is with Department of Computer Science, Kent State University, Kent, 44919, USA (e-mail: jykim2@kent.edu).

Y. Jang is with Industrial and Operations Engineering Department, University of Michigan, Ann Arbor, MI 48019, USA, (e-mail: mapsossa@umich.edu).

E. Byon is with Industrial and Operations Engineering Department, University of Michigan, Ann Arbor, MI 48109, USA (e-mail: ebyon@umich.edu).

D. M. Tilbury is with Mechanical Engineering Department, University of Michigan, Ann Arbor, MI 48109, USA (e-mail: tilbury@umich.edu).

M. Engoren is with the Department of Anesthesiology, Medical School, University of Michigan, Ann Arbor, MI 48109, USA, (e-mail: engorenm@umich.edu).

S. K. Ramachandran is Vice Chairman for Quality, Safety, and Innovation in Anesthesiology Beth Israel Deaconess Medical Center Harvard Medical School, Boston, MA 02215, USA, (e-mail: skrama@bidmc.harvard.edu).

M.S Kang is with the Department of Computer Science and Engineering, Ewha Womans University, Seoul 03760, Republic of KOREA (Corresponding Author, e-mail: mesun@ewhain.net).

thus, they have limitations in capturing abnormal respiration patterns in practice. Recently, Liu *et al.* [16] proposed channel state information (CSI)-based respiration monitoring system with the Wi-Fi devices and showed that their monitoring system could overcome the aforementioned limitations of other devices. Their study, however, has been limited to monitor RR only, and monitoring VT was not considered.

There are several challenges to estimate VT. First, there are multiple CSI subcarriers containing different quality of respiration information. In other words, some subcarriers provide more informative respiration data, whereas others provide less informative ones. Therefore, selecting an informative CSI subcarrier is critical for the quality of VT. Second, there is no ground-truth VT for comparison with the estimated VT from the Wi-Fi device, so it is hard to measure the similarity between measured and estimated VT. Third, the amplitudes of CSI signals depend on the selected subcarrier. Consider 30 subcarriers, each with 3 antennas of the receiver (RX). Among the 90 subcarrier/antenna combination (3 antennas of the RX and 1 antenna of the transmitter (TX)), the optimal subcarrier/antenna selected by the developed subcarrier selection module varies, depending on experimental environments such as positions, postures and subjects. Thus, it is difficult to calibrate the Wi-Fi monitoring for VT estimation as a sensor.

To address these issues, we propose a new respiration monitoring system to estimate the relative VT based on the initial amplitudes of the CSI signals in the commercial off-the-shelf Wi-Fi devices. The monitoring system includes the hardware device, data processing modules, and relative VT estimation algorithms. Specifically, we develop a data processing algorithm to extract relevant parameters from the Wi-Fi signal for estimating VT. We also propose a new algorithm to choose the best CSI for monitoring.

We evaluate the performance of our approach in various monitoring conditions. First, we use a human patient simulator (HPS) at different levels of VT setting. In the HPS, we vary the VT from 600 *mL* to 100 *mL* in decrements of 100 *mL* every 1 minute. Our estimation results show good agreement with the HPS setting. Next, to verify the practicability of the approach, we perform experiments with a real human subject in different sleep postures and positions, Wi-Fi router positions, and monitoring environments. In each case, the human subject varies the VT from 1000 *mL* to 250 *mL* in decrements of 250 *mL* every 1 minute and we measure the VT using a spirometer. Our monitoring results from both experiments (one with HPS and the other with the real human subject) indicate the strong performance of the proposed approach in monitoring VT. Specifically, the correlation coefficient of the relative VT between our estimations and the HPS settings is 0.99. In the real human subject test, the correlation coefficients of relative VT between our estimated and the actual VTs are between 0.93 and 0.99. The results demonstrate the robust performance of the proposed approach in monitoring the relative VT. Moreover, experimental results suggest that our approach can successfully monitor RR as well.

To the best of our knowledge, this paper is the first study to monitor the relative VT using the CSI of Wi-Fi signals. Recently some studies estimate RR using the Wi-Fi signals [16, 17] (to be detailed in Section II). However, no methods have been proposed to extract the VT information from the Wi-Fi signal. Wi-Fi devices are common in our daily life and do not need to be attached to the body. Consequently, our proposed approach has practical implications for non-invasive health monitoring. The attained results suggest high promise for non-intrusive respiration monitoring and timely detection of respiration problems.

Section II reviews related studies. Section III describes the proposed approach to estimate VT from the HPS and human subject using the CSI. Section IV presents our experimental set-up using the HPS and human subject with the commercially available Wi-Fi device. Section V describes the experiments and reports the evaluation results. Section VI discusses the used parameter for VT estimation. Section VII concludes this study and presents future research directions.

II. CSI Background and Related Work

A. *Technical Background of Channel State Information [18]*

The CSI can be described how wireless signals propagate from the TX to the RX at specific carrier frequencies and also shows the combined effects, such as scattering, fading and power decay with distance [17]. The multi-path effects, such as amplitude attenuation and phase shift, impact on CSI amplitude and phase. Each CSI entry indicates the Channel Frequency Response (CFR) including the amplitude attenuation factor, propagation delay and carrier frequency [19]. The CSI amplitude and phase are impacted by the adjacent environment, such as the physical movements of the TX, RX, objects or humans [18].

The multiple subcarriers are generated from a Wi-Fi channel with Multiple-Input and Multiple-Output (MIMO) by using the orthogonal frequency-division multiplexing (OFDM). To measure CSI values, the Wi-Fi TX transmits Long Training Fields including the pre-defined symbols for each subcarrier of the packet preamble. The Wi-Fi channel is modeled by $\boldsymbol{G_r} = C\boldsymbol{G_t} + \boldsymbol{Q_v}$, where $\boldsymbol{G_r}$ is the received signal vector in the RX, $\boldsymbol{G_t}$ is the transmitted signal vector in the TX, C is the CSI matrix, and $\boldsymbol{Q_v}$ is the noise vector, for each subcarrier. The RX checks the CSI matrix C using $\boldsymbol{G_t}$ and $\boldsymbol{G_r}$ after processing to remove cyclic prefix, demapping, and OFDM demodulation [18].

We use the CSI tool [20] built on the commercially available Intel Wi-Fi Wireless Link 5300 (IWL5300) 802.11n MIMO radios using custom modified firmware and open-source Linux wireless drivers. The IWL5300 provides 802.11n CSI in a format that reports the channel matrices from 30 subcarrier groups, which is either one group for every two subcarriers at 20 *MHz* or one group for every four subcarriers at 40 *MHz*. Each channel matrix entry is a complex number with the signed 8-bit resolution for both the real and imaginary parts and specifies the gain and phase of the signal path between a single transceiver antenna pair.

The CSI tool records detailed measurements of the wireless channel along with received 802.11 packet traces. It runs on a commodity 802.11n network interface card and records CSI based on the 802.11n standard [21]. The CSI contains information about the channel between the TX and RX at the level of individual data subcarriers. Our system uses the Intel Wi-Fi Link 5300 wireless network interface card with three antennas. In our experiment, we use Ubuntu 10.04 LTS with the 2.6.36 kernel on a Dell Latitude E5520 Laptop with Intel core i5-25s0M (2.5 *GHz*). We install customized versions of Intel's closed-source firmware, open-source *iwlwifi* wireless driver, userspace tools to enable these measurements, access point functionality for controlling both ends of the link, and MATLAB 2014 for data analysis.

B. Related Work

Several studies estimate respiratory parameters using different types of contact devices including electrocardiogram, strain gauge, accelerometer, pressure, piezoelectric belt, and pulse oximetry [14]. However, due to their inconvenience, people tend to prefer monitoring respiratory parameters using less obtrusive and non-contact type devices. Overall, the non-contact respiration monitoring systems can be categorized into three main types: systems using microphones, systems using vision type sensors, and systems based on RF signals.

First, monitoring systems using microphones usually locate microphones near patients in a quiet environment. Que *et al.* [5] propose a VT and RR estimation method using tracheal breath sounds. Although this method can detect deep and low pitched breath sounds, the sound of the airflow should exceed the background noise. Therefore, this monitoring method is not useful in noisy environments.

Second, monitoring systems that employ vision type sensors can provide relatively straightforward information. Lewis *et al.* [15] use the infrared video recording of the face during a variety of respiratory conditions to extract breath-to-breath timing intervals. They track the relative VT from thermal videos of the nostril region. However, it performs poorly when a subject's head is moved out of the infrared video angle. Transue *et al.* [1] propose a vision-based technique to monitor VT based on a three-dimensional (3D) chest surface reconstruction using a depth camera. They apply the 3D space-time volumetric representation in order to generate omni-directional deformation states of the chest size change associated with VT. Although this technique uses a depth-camera like Kinect, privacy concerns still remain. In fact, both microphone (the first monitoring method) and vision based sensors (the second monitoring method) cause potential privacy concerns to users.

Finally, respiration monitoring systems using RF signals exhibit many advantages of being unobtrusive, having no light interruptions and fewer privacy concerns. Existing studies in the literature have used three RF technologies: RSS, radar type, and CSI from Wi-Fi device. Among the three RF technologies, RSS has been widely used for capturing respiration signals. Patwari *et al.* [22] and Patwari *et al.* [23] measure the RSS from a network using commercial off-the-shelf wireless transceivers. Abdelnasser *et al.* [24] propose a method to extract the breathing signal from a Wi-Fi RSS using a commercial off-the-shelf device for detecting sleep apnea. Kaltiokallio *et al.* [25] use a single TX and RX pair to identify RR using RSS and compute RR in different lying positions. However, the RSS is not sensitive enough to track small chest movements reliably. According to De Groote *et al.* [26], the primary movement of the chest is between 3mm and 5mm. These small changes are

TABLE I

COMPARISON OF PREVIOUS STUDIES USING UNOBTRUSIVE MONITORING METHODS WITH THE PROPOSED MONITORING METHOD

Reference	Device type	Privacy Concern	Monitoring Respiration Rate	Monitoring Tidal Volume
Proposed monitoring system	**CSI**	**No**	**Yes**	**Yes**
Que *et al.* [5]	Microphone	Yes	No	Yes
Transue *et al.* [1]	Vision (Depth camera)	Yes	Yes	Yes
Lewis *et al.* [15]	Vision (Infrared video)	Yes	Yes	Yes
Patwari *et al.* [22]	RF signal (RSS)	No	Yes	No
Patwari *et al.* [23]	RF signal (RSS)	No	Yes	No
Abdelnasser *et al.* [24]	RF signal (RSS)	No	Yes	No
Kaltiokallio *et al.* [25]	RF signal (RSS)	No	Yes	No
Adib *et al.* [28]	RF signal (FMCW)	No	Yes	No
Nguyen *et al.* [29]	RF signal (Directional radio)	No	No	Yes
Wang *et al.* [30]	RF signal (CSI)	No	Yes	No
Liu *et al.* [16]	RF signal (CSI)	No	Yes	No
Lie *et al.* [17]	RF signal (CSI)	No	Yes	No
Liu *et al.* [27]	RF signal (CSI)	No	Yes	No

easily disturbed by environmental noise and human activities. The RSS signals, which take integer values in a narrow range between -20 *dB* to -17 *dB,* cannot distinguish such small chest movements from noise and disturbances [27]. To address the low sensitivity and low resolution of RSS signals, respiration monitoring based on RSS measurements typically assumes a periodic breathing pattern and converts the original integer-valued signals to sinusoidal signals. [17, 27]. However, such treatment does not capture abnormal breathing patterns, e.g., sleep apnea, that do not follow the periodic pattern, making the monitoring results less accurate.

Adib *et al.* [28] use a frequency modulated continuous wave (FMCW) radar technique to monitor respiration and heart rate based on a signal sweeping from 5.46 *GHz* to 7.25 *GHz* every 2.5 milliseconds with transmitting sub-*mW* power. This technique is also useful to detect the human breath through-wall. Nguyen et al. [29] use a phase-motion demodulation algorithm to monitor breathing volume based on the fixed directional radio devices placed above the subject. These Vital-Radio technique and directional radio are, however, of low practical utility [17], because they require expensive hardware.

Wi-Fi devices have great potential to be a practical solution for tracking individuals' breathing patterns in smart homes or clinical settings. Unlike RSS, Liu *et al.* [16] use the CSI from the Wi-Fi devices to monitor respiration to detect suppressing breath. They apply the CSI system in a home environment to monitor RR. However, their study [16] as well as the studies by Liu *et al.* [17], Wang *et al.* [30], and Liu *et al.* [27] track the RR with simple and artificial sleep apnea events and do not monitor the VT. Table 1 summarizes the previous methods to monitor and estimate the respiratory parameters in an unobtrusive way and compares them to our proposed monitoring system.

We would like to highlight the novelty of our study, compared with existing methods. Unlike previous studies that estimate RR only using the CSI in the Wi-Fi signal [16, 17], our approach can estimate both VT and RR, extracting richer information from the signal. Compared with the RSS monitoring method, CSI represents fine-grained physical layer information which has much higher sensitivity and resolution than RSS [17], enabling us to capture small chest movements, e.g., less than 5 *mm* which corresponds to VT of about 600 *mL* (see Section V) [26] and to track both normal and abnormal breathing (see Section VI).

III. Wi-Fi Monitoring System

The proposed approach can estimate both VT and RR using the CSI in commercial off-the-shelf Wi-Fi signals. Because the focus of this study is to estimate VT, this section discusses the VT estimation method, while the method for estimating RR and implementation details are summarized in Appendix A.

A. Overview of monitoring procedure

The main idea of our approach is to extract the relative VT from the chest movement. Fig. 1 summarizes the overall procedure. The monitoring system captures time-series of CSI amplitude measurements collected by the Wi-Fi device with three antennas using system-generated 156 *Hz* traffic (sampling rate). It includes 30 subcarriers, each with 3 antennas collecting measurements in 156 *Hz*. As such, the input becomes 30-by-3 matrix called as CFR matrix collected in 156 *Hz*, as shown in Fig. 1. The captured raw CFR signals are preprocessed to get clear signals and obtain the frequency domain information for selecting the best subcarrier.

After preprocessing, the Subcarrier Selection module is applied to select the best CSI data among the 90 subcarrier/antenna using 90 Power Spectrum Densities (PSDs) as a frequency domain (see Section III.D.). After selecting the best subcarrier, the Peak and Valley Detection as a time domain finds the local maxima and minima of the signal using the MATLAB ‘findpeaks’ function with the minimum peak width of 1.15 seconds. The Fake Peak/Valley Filtering module removes the outliers from the extracted peaks and valleys (see Appendix D). Finally, the Parameter Estimation extracts the features regarding the filtered peaks and valleys for RR / Relative VT Estimation.

B. CSI Collection [17]

The monitoring system, including the RX with three antennas and the TX with one antenna, captures 156 packets per second as shown in Fig 1. Each packet includes 30-by-3 (CFR) matrix. Each column and row of the CFR matrix indicates one antenna and one subcarrier, respectively. The CFR with the i^{th} column of the matrix extracted from the j^{th} packet received can be written as

$$CFR^i(j) = \left[F_1^i(j), F_2^i(j), \ldots F_{30}^i(j)\right]^T \quad (1)$$

where $F_k^i(j)$ is the CFR on the k^{th} subcarrier at time instant j of antenna i. The $F_k^i(j)$ is a complex number and is represented by the amplitude $|F_k^i|$ and the phase δF_k^i as $F_k^i = |F_k^i| * e^{\delta F_k^i}$. In order to process the time-series information of $CFR^i(j)$, the

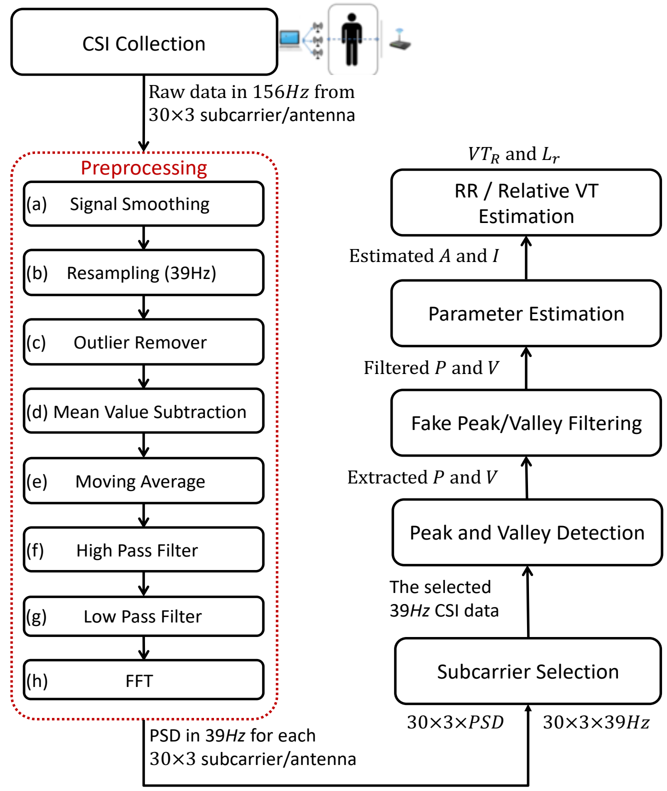

Fig. 1. Overall procedure to estimate the relative VT and RR.

CFR^i includes 30-by-n is calculated by:

$$CFR^i = [CFR^i(1), CFR^i(2), \ldots CFR^i(n)] \quad (2)$$

where n is the number of packets received at antenna i. Each row of CFR^i indicates the temporal change of the CSI information over one subcarrier so that we use the amplitudes of CFR^i for the input of the preprocessing.

C. Preprocessing

The preprocessing procedure consists of eight steps (in Fig. 1) to extract the PSDs in frequency domain for selecting the best subcarrier and extract clean time-series signal for estimating relative VT.

(a) Signal smoothing: A moving average filter is used for signal smoothing to filter out the initial high frequency. We use M^{th} order moving average filter that sequentially takes average values of last m data, $CFR^i(t)$, $CFR^i(t-1)$, ⋯, $CFR^i(t-m+1)$, so that the filtered data at time t, Y_t^i, can be estimated by

$$Y_t^i = \frac{1}{m}\sum_{l=0}^{m-1} CFR^i(t-l). \quad (2)$$

(b) Resampling: We uniformly resample the smoothed signal from 159 *Hz* ($\boldsymbol{Y}_{159Hz}^i$) to 39 *Hz* ($\boldsymbol{Y}_{39Hz}^i$) for reducing the computation.

(c) Outlier removal: A typical Wi-Fi signal includes outliers such as a deep valley that significantly deviates from the normal pattern. If we blindly apply common filtering methods without removing outliers, the resulting amplitude becomes inaccurate. We identify such outliers based on the empirical distribution of

This article has been accepted for publication in a future issue of this journal, but has not been fully edited. Content may change prior to final publication. Citation information: DOI 10.1109/JSEN.2020.3023178, IEEE Sensors Journal

Algorithm 1: An algorithm for Outlier Removal

Input: Data Array CSI_DATA
Output: Data Array CSI_DATA_Result

a. Check all angles between adjacent data points (S_Agl) and save into array variable (S_Agl_Arr).
b. S_Mean = Averaging the dt_fTh
c. S_STDEV = square root (S2)
d. Rms_3delta = S_STDEV * 3
e. dt_th = S_Mean + Rms_3delta

```
for CSI_DATA[i] from 2 to length(CSI_DATA) by 1
  S_Agl = (CSI_DATA(i) - CSI_DATA(i - 1));
  S_Agl_Arr(i) = S_Agl;
  if (S_Agl < 0) & (abs(S_Agl) > abs(dt_th))
   CSI_DATA_Result(i) = dt_WiFi_P;
    if flag_check_i == 0
      flag_check_i = 1;
    end-if
    S_Agl_1 = CSI_DATA(i);
  else if flag_check_i == 1
      CSI_DATA_Result(i) = CSI_DATA(i) - (S_Agl_1 - S_Agl);
      S_Agl_2 = CSI_DATA(i);
      if (dt_WiFi >= 0) & (abs(dt_WiFi) > abs(dt_th))
        flag_check_i = 0;
        CSI_DATA_Result(i) = S_Agl_2 + abs(S_Agl_1 - S_Agl);
      end
      else if (dt_WiFi >= 0) & (abs(dt_WiFi) > abs(dt_th))
        CSI_DATA_Result(i) = S_Agl_2 + abs(S_Agl_1 - S_Agl);
      else
      CSI_DATA_Result(i) = CSI_DATA(i);
      dt_WiFi_P = CSI_DATA(i);
      end-if
    end-if
  end-if
end-for
```

the Wi-Fi measurements and remove the outliers with the sudden Wi-Fi signal amplitude graph's angle changes.

Specifically, let d_i denote the differential value of Wi-Fi signal, $\boldsymbol{Y}^{i}_{39\,Hz}$, and W denote the number of measurements. We obtain the sample mean, $\bar{d}$, and the sample standard deviation, s, as

$$\bar{d} = \frac{1}{W}\sum_{i=1}^{W} d_i, \tag{3}$$

$$s = \sqrt{\frac{1}{W-1}\sum_{i=1}^{W}\left(d_i - \bar{d}\right)^2}\,. \tag{4}$$

Then, we set the threshold value as $\bar{d} + 3s$, so that d_i is marked as an outlier when $|d_i|$ exceeds this threshold, i.e.,

$$|d_i| > \bar{d} + 3s. \tag{5}$$

With this threshold, about 0.3% of data is identified as outliers when the differentials are normally distributed. Even for non-normal distributions, this threshold can be practically applied for removing outliers [31] and the removed signal is represented as $\boldsymbol{R}^i$. The detailed pseudo code of the outlier removal algorithm is shown in Algorithm 1.

Then, we employ commonly used filtering techniques:

(d) Mean value subtraction:

$$Z_t^i = R_t^i - \overline{R_t^i}, \tag{6}$$

where $\overline{R_t^i}$ is the average value of R_t^i at i^{th} antenna.

(f) Moving average: 5th order moving average to reduce high-frequency noise.

(g) High pass filter: High pass filter (with 0.01 *Hz* cut-off frequency) to prevent a drift suppression.

(h) Low-pass filter: Low-pass filter (with 0.6 *Hz* cut-off frequency) to suppress the high-frequency information even more. F_t^i is the filtered value using (f, g, h) from Z_t^i. We use the 'filtfilt' function for high/low-pass filter in the MATLAB.

(i) Fast Fourier Transform: We use Fast Fourier Transform (FFT) to convert the preprocessed time-series signal, F_t^i, to the frequency domain to generate features for selecting the best-effort signal quality. We use the 'fft' functions for FFT, respectively in MATLAB.

Fig. 2 shows the preprocessing effects including signal smoothing, resampling, outlier remover, mean value subtraction, and filtering processes (moving average, high/low pass filters) to filter out various noises or artifacts. As can be seen, the preprocessing improves the signal quality for respiration monitoring.

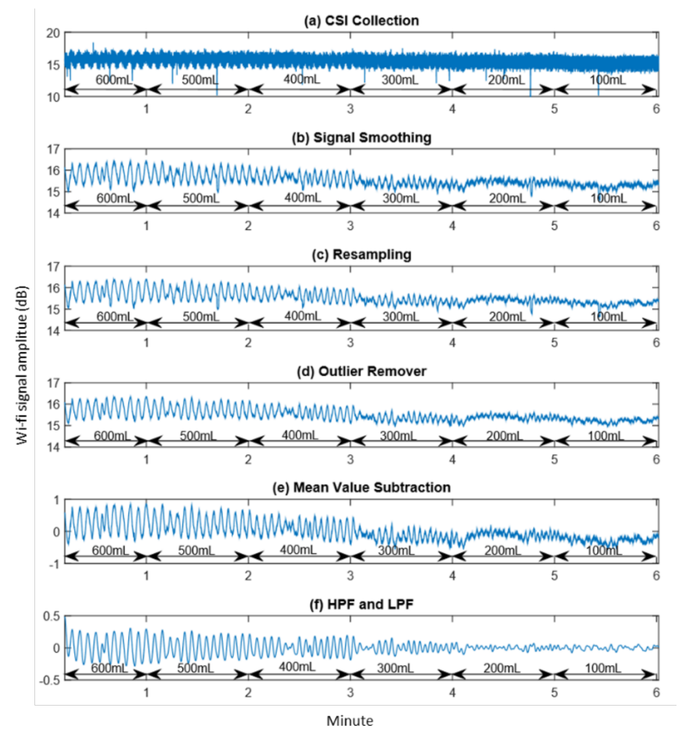

Fig. 2. Preprocessing effects

D. Subcarrier Selection

Among the 90 CSI data available in the CSI tool, some subcarriers provide high-quality breath signals, whereas others provide less useful information. Typically, breathing frequency from child to adult ranges 8 min^{-1} ~ 37 min^{-1}, which corresponds to the range of RR, 0.133 *Hz* ~ 0.633 *Hz*. Fig. 3 shows the frequency domain power spectral density. When the subcarrier successfully measures human breaths, the power spectral density in FFT includes a high amplitude peak in the frequency range of 0.133 *Hz* ~ 0.633 *Hz* (see Fig. 3) (we denote this range as α). Moreover, when the breath information in the subcarrier is clearly collected, the amplitudes in other frequency ranges, i.e., 0.633 *Hz* ~ 1.047 *Hz* (denoted as β) are low, as shown in Fig. 3.

This article has been accepted for publication in a future issue of this journal, but has not been fully edited. Content may change prior to final publication. Citation information: DOI 10.1109/JSEN.2020.3023178, IEEE Sensors Journal

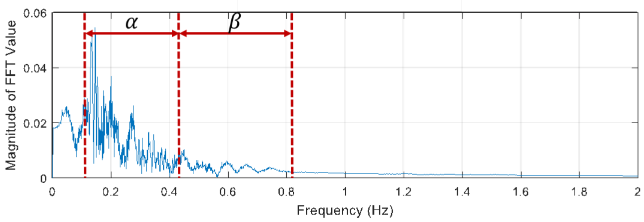

Fig. 3. Example of power spectral density of FFT.

In order to select the best subcarrier/antenna that provides high amplitude signals of typical breath with low artifacts, our subcarrier selection module captures two values: the maximum amplitude of α, denoted as α_M, and average value of β, denoted as β_A. Signals from a good subcarrier with clear respiration and minimum noise should have high amplitude peak and small noise. In other words, a good subcarrier results in a large α_M and small β_A. Therefore, we use the ratio of α_M to β_A, referred to as the relative breath amplitudes, R, as follows.

$$R = \alpha_M / \beta_A \tag{7}$$

Then we choose the subcarrier with the largest R value.

E. Peak/valley detection and fake peak/valley detection

We extract all peaks and valleys in the selected respiration signal using the local maxima and minima approach. The algorithm finds all the peaks and valleys having widths of at least 39 samples (one second). Among the extracted data, fake peak/valley is filtered based on the range of breathing frequency ($8\ min^{-1} \sim 37\ min^{-1}$). These processes provide the initial parameters to the parameter estimation module.

F. Parameter estimation and relative VT Estimation

We note that VT is related to the lung space volume of the human body, which is defined as the range of amplitude oscillation at each breath [15]. Therefore, we extract the amplitude (associated with lung space volume) from body reflection.

The respiratory amplitude can be calculated as the difference between the peak value and its adjacent valley in the Wi-Fi CSI signal. Considering that there are two adjacent valleys for each peak in the signal, we subtract the average of the two adjacent valleys from the peak value to get each amplitude. Specifically, at the j^{th} $(j = 1, 2, \cdots, J)$ time window, we obtain the k^{th} amplitude, PV_k^j, as

$$PV_k^j = P_k^j - \frac{V_k^j + V_{k+1}^j}{2} \tag{8}$$

where P_k^j and V_k^j denote the k^{th} $(k = 1, 2, \cdots, K_j)$ peak and valley, respectively, and K_j is the number of peaks/valleys in the j^{th} window. Fig. 4 shows an example of the j^{th} windows with peaks (red '*') and valleys (blue 'o') of the Wi-Fi signal including the k^{th} peak and valley. The resulting PV_k^j implies an instant amplitude at each breath.

Even when the target VT is maintained at the same level, the amplitude can slightly vary breath by breath. As such, we average instant amplitudes to get the local VT as

$$T_j = \frac{\sum_{k=1}^{K_j} PV_k^j}{K_j}. \tag{9}$$

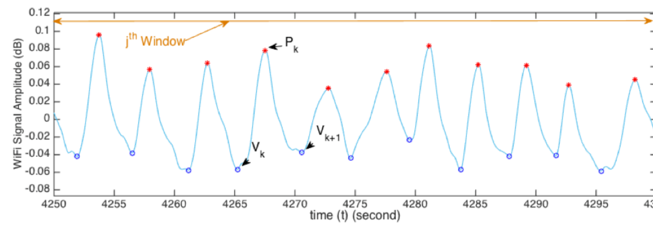

Fig. 4. Wi-Fi signal with peaks (red '*') and valleys (blue 'o')

In our experiments, we set the window segment at 20 seconds length with 5 seconds sliding step. Then, we take the average, denoted by E_h, of multiple $T_j's$ obtained at the same target VT level. Because the amplitudes of the extracted Wi-Fi signals vary from subcarrier to subcarrier, following the procedure in [14], we obtain the relative VT, VT_R, by normalizing E_h with its initial VT, E_0, i.e.,

$$VT_R = \frac{E_h}{E_o} \times 100. \tag{10}$$

Note that to the best of our knowledge this is the first study that tackles the challenges of relative VT estimation. We estimate the relative VT from CSI signals and compare it with the ground truth VT measured from HPS and a human subject, whereas the existing methods using CSI signals [16, 17, 27, 30] estimate the respiration rate only due to the difficulties of measuring the ground truth VT.

IV. Experimental Setting

To verify our proposed approach, we conducted experiments using HPS and with a real human subject. Since HPS provides accurate and constant VT values based on the predefined setting, it can be used for verifying measuring accuracy. In the experiments with a human subject, we employ diverse measuring environments, such as sleep postures or positions, for checking practical usability. This section explains our experimental setting and procedure in detail.

A. System Setting for Human Patient Simulator (HPS)

HPS is an electronic mannequin-type physical simulator that can simulate inhalation and exhalation functions with actual chest movements (Fig. 5(a)). It is designed for simulating anesthesia and respiratory functions with respiratory modeling and lung mechanics [32]. The size of the HPS mannequin used in our experiment is 180 *cm* in height and weighs 34 *kg*, and the outer material is latex. Fig. 5 shows the experimental setting using a Linux laptop with the Intel 5300 NIC board and open-case three antennas, HPS mannequin, and Wi-Fi router with one antenna.

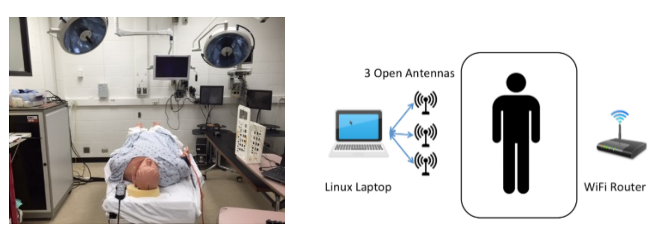

(a) HPS test environment (b) Schematic of test environment

Fig. 5. Overview of experiment setup

This article has been accepted for publication in a future issue of this journal, but has not been fully edited. Content may change prior to final publication. Citation information: DOI 10.1109/JSEN.2020.3023178, IEEE Sensors Journal

Using HPS, we can manually set the target VT value. Ideally, the target value should match with the actual value of the mannequin. In reality, the actual VT in HPS can be slightly different from their set values (i.e., the target VT). After the target value is set, the HPS physiological model tunes the actual value toward the target value. In this process, the actual value can slightly deviate from the target value for a steady state and the HPS automatically adjusts its chest excursions to produce the VT close to its set value.

In general, an actual VT can be measured by using a Wright spirometer connected to either an endotracheal tube or with a tight mouth seal. However, the physical structure of the mannequin precluded use of a tightly sealed Wright spirometer. Therefore, when we evaluate the VT estimation accuracy, we use the set value as ground truth VT value.

Recently the research of the Fresnel zone model, which determines the quality of extracted Wi-Fi signals based on the series of concentric ellipsoids of alternating strength, was performed to find the right environmental setting [30, 33]. Their researches suggest that the closer a subject is to the line between TX and RX devices, called the line-of-sight (LOS), the clearer periodic patterns can be obtained, and when a subject is 2 meters away from the LOS, respirations cannot be detected. Additionally, the LOS distance should not be larger than 3 meters. We select the environmental setting according to the conditions suggested in [30, 33].

Fig. 6 illustrates the detailed configuration including the distances between devices and HPS. We set the TX (Wi-Fi router antenna) and RX (three antennas of the Linux laptop) 190 cm apart, and place the center of the HPS mannequin 80 *cm* from the RX antenna and 50 *cm* from the head to the centerline (the line between RX antenna 2 and TX antenna). The distances between mannequin's chest and floor and between the antennas and floor are 104 *cm* and 105 *cm*, respectively.

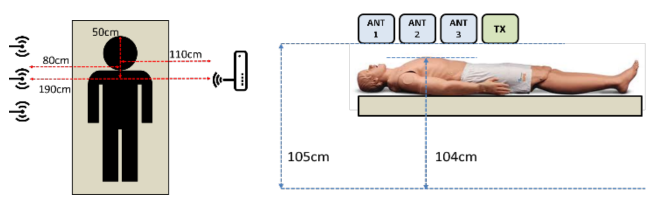

(a) top view (b) side view

Fig. 6. HPS and Wi-Fi system setting configuration

B. System Setting for Human Subject Test

To validate our proposed method's practicability, we also conduct experiments with a real human subject in various measuring environments, including different sleep postures, sleep positions, Wi-Fi routers' positions, and room size. The human subject is 174 *cm* tall and reclined on a bed, trying to breathe with VT from 1000 *mL* to 250 *mL* in decrements of 250 *mL* every 1 minute using a spirometer to measure and maintain the target VT level every minute. We also measure actual VT values using the spirometer.

We consider several experimental settings as shown in Fig. 7. Fig. 7(a) shows four different sleep postures including starfish, log (or lateral decubitus), soldier (or supine), and fetal. Fetal is the sleep position curled-up lying on one side. Log is the sleep position lying on side with both arms down and keeping the spine straight. Soldier is the sleep position lying on back with arms down close to body, and starfish is the sleep position lying on back with both arms up near sleeper's head. Fig. 7(b) depicts three sleep positions (O1: left, O2: middle, O3: right) in the bed. Fig. 7(c) illustrates the detailed configuration including different locations of RX that are marked as circled numbers 0, 1, and 2 (T0, T1, and T2 respectively). Heights of bed, RX (ANTs), and TX are 53 cm, 83 cm, and 65 cm, respectively. The distance between RX (ANTs) and T1 is 168 cm and T0 is located in the same distance away from the RX (ANTs) horizontally and 10 cm away from the top of the bed vertically. T2 is located 212 cm away from the top of the bed vertically and 84 cm away from the RX (ANTs) horizontally. Fig. 7(d) represents the details of the room structure. The experiments with the combinations of these setting are separately conducted in both living room and bedroom.

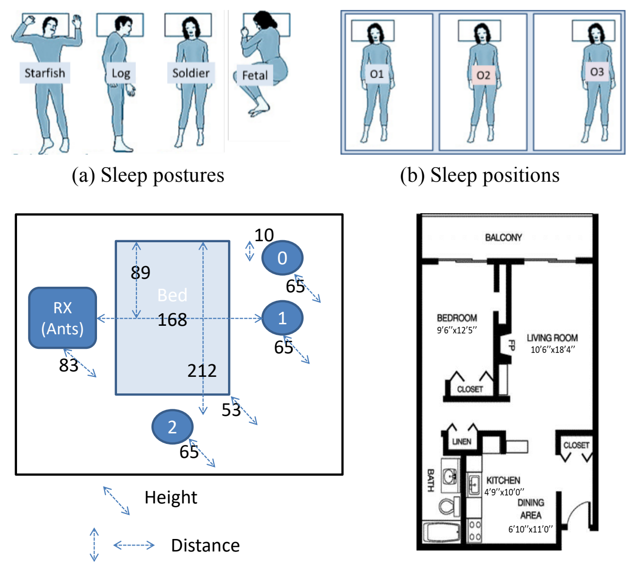

(a) Sleep postures (b) Sleep positions

(c) Wi-Fi system setting configuration (Unit: cm) (d) Floor plan

Fig. 7. Human subject test factors

V. Experimental Results

This section presents the results of the proposed approach from our experiments with the HPS system and real human subject.

A. Relative VT Estimation in HPS

To evaluate the estimation accuracy of the proposed approach at different VT levels, we change the target level of VT every minute. Specifically, we set the VT of HPS sequentially at 600 *mL*, 500 *mL*, 400 *mL*, 300 *mL*, 200 *mL* and 100 *mL*. Fig. 8 depicts the processed time-series signals of Wi-Fi along with VT settings in the HPS (see the number above the arrow). We can see that the amplitudes and intervals of the Wi-Fi signal successfully reflect the VT changes.

To evaluate the estimation performances of the method, Fig. 8 provides the comparison between the estimated VTs (i.e., VT_R in (7)) and VT set values at different levels.

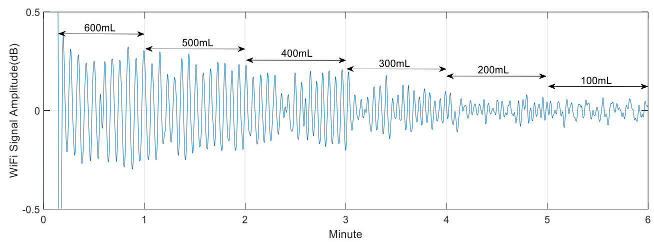

Fig. 8. Experimental result of the processed Wi-Fi signal at different levels of VT (note: each number above the arrow indicates the VT setting on HPS system).

To evaluate the impact of the FFT time window on the estimation performance, we compare the six relative VT values between Wi-Fi measurements and HPS settings. Table II summarizes the correlation coefficients with different FFT time windows of the HPS test, demonstrating that the estimation performance is not sensitive to the FFT window size.

TABLE II
Relative VT estimation performance with different FFT window sizes using HPS

FFT Window Size	60s	120s	180s	360s
Correlation	0.98	0.99	0.97	0.99

In general, the estimated results are close to the HPS set values, demonstrating the strong estimation performance of our approach. The correlation coefficient between the HPS settings and the estimated VTs using Wi-Fi is 0.99. These results indicated that our method which uses the amplitude information from the Wi-Fi signal captures the lung volume of the human body well, which leads to accurate VT estimation.

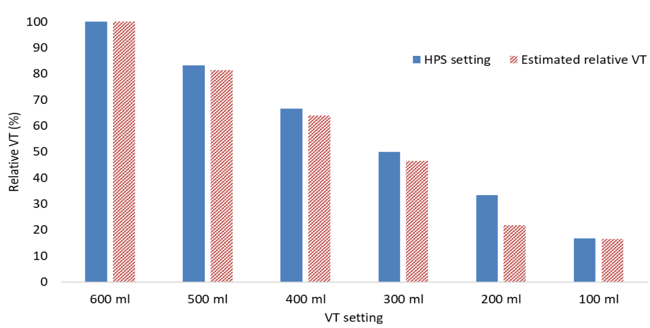

Fig. 9. Comparison between the estimated relative VTs based on Wi-Fi signal (left, blue-solid column) and the actual relative VT in HPS setting (right, red-dashed column).

We observe in Fig. 9 a slight mismatch between our estimations and the set value, especially when the VT is set at 200 *mL* in the HPS. As we discussed earlier, the actual VT of the mannequin in the HPS system can be different from the set value. Therefore, our estimation mismatch might be partially due to the discrepancy between the actual VT and set value. Another reason might be due to the material of HPS. The outer covering of the HPS used in this study is latex, which is different from human skin. Wilson [34] reports the reflection and transmission losses through different materials, concluding that the transmitted and reflected energy of the Wi-Fi signal can be affected by different materials. Specifically, the human body consists of about 60% water for men and about 50% for women [35], which is different from the latex shell of the HPS. Liu *et al.* [16] also report fake peaks which are the identified peaks in the different locations of actual peaks of the sinusoidal CSI amplitude pattern on the human body. The latex material possibly makes this issue worse. Despite the slight mismatch at the set value of 200 *mL,* considering that the normal VT is 5 to 7 *mL* per *kg* of ideal human body weight, 200 *mL* of VT is generally observed from people with the weight of 30 to 40 kg, which is small for adults. Therefore, our method would still be clinically useful for estimating VTs for adults.

B. *Relative VT Estimation with a Real Human Subject*

We additionally evaluate the accuracy of the relative VT from the experiments with a human subject in a real environment. We conduct experiments with different sleep postures, sleep positions, Wi-Fi router's positions, and rooms.

Fig. 10 shows the sample resulting signal graph in the setting (soldier sleep posture, O2 sleep position, T1 router position, and Bedroom). At each experiment, the human subjects changed the target level of VT every minute, sequentially 1000 *mL*, 750 *mL*, 500 *mL*, and 250 *mL*. Although the human subject tried to maintain the constant VT at each minute, there were small variations in the actual VT. As such, direct comparisons between the estimated values with the target levels would be less meaningful, different from the experiment with HPS where we can control actual VT levels. Instead, we take the mean spirometer measurements during 1 minute and use this mean value as ground truth. The upper arrow in each graph denotes the 1-minute mean spirometer VT measurement.

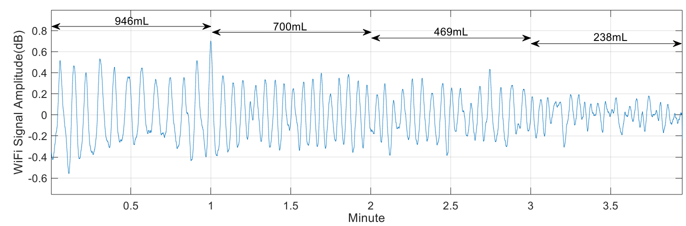

Fig. 10. The resulting signal graph in the human subject test with conditions, such as Soldier sleep posture, O2 sleep position, T1 router position and Bedroom.

Then, to measure the estimation accuracy, we obtain the correlation coefficients between the estimated values and the spirometer average measurements. Table III summarizes the correlation coefficients obtained from experiments in different settings. The best result is obtained at the combination of starfish, O2, T1, and bedroom with correlation coefficient close to 1. In the sleep posture, starfish performs the best, but the other three sleep postures also achieve high correlation coefficients. Regarding the sleep position, O2 is slightly better than O1 and O3. In addition, our experiment performed in the bedroom shows a better result than that in the living room. For the Wi-Fi router position, T1 generally performs better than other positions. Overall our analysis suggests that our estimation performance is consistently strong and robust to a variety of sleeping and environmental factors.

The reason that the correlation coefficients in the human subject experiments are slightly lower than those in the HPS experiments is that the human subject could not keep the VT at a constant level over each minute. For example, during the experiment, unexpected outlier breaths occurred easily.

This article has been accepted for publication in a future issue of this journal, but has not been fully edited. Content may change prior to final publication. Citation information: DOI 10.1109/JSEN.2020.3023178, IEEE Sensors Journal

However, the results show the potential of our approach to monitor VT in real living environments.

TABLE III
THE RESULT OF THE REAL HUMAN SUBJECT TEST IN DIFFERENT ENVIRONMENTS

Sleep Posture	Sleep Position	Wi-Fi Router Position	Room	Correlation Coefficient
Soldier	O2	T1	Bedroom	0.97
Fetus	O2	T1	Bedroom	0.99
Starfish	O2	T1	Bedroom	1.00
Log	O2	T1	Bedroom	0.99
Soldier	O1	T1	Bedroom	0.97
Soldier	O2	T1	Bedroom	0.99
Soldier	O3	T1	Bedroom	0.97
Soldier	O2	T0	Bedroom	0.94
Soldier	O2	T1	Bedroom	0.97
Soldier	O2	T2	Bedroom	0.99
Soldier	O2	T1	Living Room	0.93
Soldier	O2	T1	Bedroom	0.97

We compare the four relative VT values of the human subject (1000 ~ 250 *mL*) between Wi-Fi measurements and diverse settings. Table IV summarizes the correlation with different FFT time windows of the human subject tests. The estimation performance is comparable, except one case with the FFT window size of 60 seconds.

TABLE IV
RELATIVE VT ESTIMATION PERFORMANCE WITH DIFFERENT FFT WINDOW SIZES WITH HUMAN SUBJECT

FFT Window Size	60s	120s	180s	360s
Correlation	0.8	0.95	0.91	0.99

VI. DISCUSSION

This study uses various methods and parameters to estimate relative VT due to the characteristics of CSI.

It is worthwhile to highlight the advantage of the proposed subcarrier selection algorithm over the methods proposed in the literature [16, 27]. Liu *et al.* [16] claim that the low-index subcarriers provide better monitoring results. However, our implementation shows that monitoring performance does not relate to the subcarrier index. This is because subcarriers can generate good respiration signals when the human chest is located in the middle of the Fresnel zone, that is, good subcarriers depend on the position of the human chest. In our implementation, the estimation accuracy using the low index subcarrier could be more than 50% worse than that from our approach. Also, Lie *et al*. [27] propose a different subcarrier selection method using the periodicity based on the recurrence plot [36] and singular value decomposition. Our implementation results from a variety of settings suggest that the subcarrier selected by our algorithm is identical to that from the method in [27]. However, our method is much simpler and faster to implement, and also intuitive because it is based on human's breathing frequency.

It is possible to use signals from multiple subcarriers. However, from our implementation, we note that the selected best subcarrier contains the major important information while the information from the remaining 89 CSI data may be redundant or possibly reduce the estimation performance due to wrong peak and valley waveforms in the signals. Thus, in our analysis, we use the information obtained from the best subcarrier.

We also extracted the parameters of peaks and valleys from the respiration signals and calculated the averaged amplitudes. Although the target VT is maintained at the same level, the measured amplitudes can slightly different breath by breath. This is because we average all the amplitudes in the local window. Additionally, a typical Wi-Fi signal includes outliers such as a deep valley that significantly deviates from the normal pattern. If we blindly apply common filtering methods without removing outliers, the resulting amplitude becomes inaccurate. These processes are essential to estimate relative VT using CSI.

VII. CONCLUSION AND FUTURE WORK

This study presents a new unobtrusive monitoring system using a commercial off-the-shelf Wi-Fi device to estimate the relative VT. We develop a data processing method to extract the respiration features to estimate the relative VT from the raw CSI signal. We also devise the subcarrier selection module to identify the best subcarrier/antenna combination that can capture respiration patterns clearly. To verify the estimation accuracy of the proposed monitoring system, we compare our estimation results with HPS settings at various VT values. We also conduct a real human subject test and compare the proposed estimation results with the spirometer at various VT values. The proposed monitoring system achieves a high correlation coefficient of the relative VT between our estimations and the HPS settings at the level of 0.99. In the real human subject test, the correlation coefficients of relative VT between our estimations and the actual VTs range between 0.93 and 0.99. Although this study focuses on the VT estimation, our monitoring approach can also estimate the RR (see Appendix A).

The proposed approach will provide a comfortable sensing environment for people at home or in the hospital due to its unobtrusive and non-invasive characteristics. Moreover, it can be widely applicable in practice as Wi-Fi systems become more popular in many places in modern society. Future work will include detecting different types of breathing disorders. Fig. 11 shows our preliminary results with HPS for the simulated abnormal breathing case due to apnea. We can see that the CSI can capture the sleep apnea event successfully. In the future, we plan to conduct experiments under different apnea events and evaluate our estimation performance through both HPS and more human subject tests.

Moreover, considering that Wi-Fi based respiration monitoring is very sensitive to the positions of TX-RX devices, we plan to develop the system controlling the distance and height of TX-RX in order to find the optimal Fresnel zone for obtaining the best effort CSI signal.

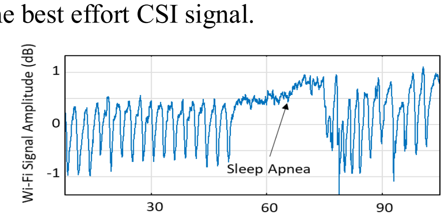

Fig. 11. Respiration signals including sleep apnea event in HPS.

REFERENCES

[1] S. Transue, P. Nguyen, T. Vu and M. H. Choi, “Real-time Tidal Volume Estimation using Iso-surface Reconstruction,” *in Proc. IEEE 1st Conf. Connected Health: Applicat. Syst. Eng. Technologies* (*CHASE*), 2016, pp 209-218, Washington DC, USA

[2] Y. Mizobe, H. Aoki and K. Koshiji, “Proposal on Nonrestraint Pulmonary Function Test Using Active 3D Measurement for Body Surface,” *in Proc. World Congr. Medical Physics and Biomed. Eng.*, vol. 2, 2007, pp. 849–852.

[3] M. C. Yu, J. L. Liou, S. W. Kuo, M. S. Lee and Y. P. Hung, “Noncontact respiratory measurement of volume change using depth camera,” *in Proc. Annu. Int. Conf. IEEE Eng. Medicine & Biology Soc.* (*EMBC*), 2012, pp. 2371-2374, San Diego, CA.

[4] C. Li, J. Ling, J. Li and J. Lin, “Accurate Doppler radar noncontact vital sign detection using the RELAX algorithm,” *IEEE Trans. Instrum. Meas.*, vol. 59, no. 3, pp. 687–695, Mar. 2010.

[5] C. L. Que, C. Kolmaga, L. G. Durand, S. M. Kelly and P. T. Macklem, “Phonospirometry for noninvasive measurement of ventilation: methodology and preliminary results,” *J. Appl. Physiol.*, vol. 93, no. 4, pp. 1515-1526, Oct. 2002.

[6] A. Bulanova, E. Bukreeva, O. Nikiforova and J. Kistenev, “The analysis of breath air by laser spectroscopy method for diagnosis of COPD,” *European Respiratory J.*, vol. 44 (no. suppl 58), pp. 1004, 2014.

[7] L. Boccanfuso and J. M. O'Kane, “Remote measurement of breathing rate in real time using a high precision, single-point infrared temperature sensor,” *in Proc. 4th IEEE RAS & EMBS Int. Conf. Biomed. Robotics & Biomechatronics* (*BioRob*), 2012, pp. 1704-1709, Roma, Italy.

[8] P. K. Dehkordi, M. Marzencki, K. Tavakolian, M. Kaminska and B. Kaminska, “Validation of respiratory signal derived from suprasternal notch acceleration for sleep apnea detection,” *in Proc. Annu. Int. Conf. IEEE Eng. Medicine & Biology Soc.* (*EMBC*), 2011, pp. 3824-3827, Boston, MA, USA.

[9] T. Reinvuo, M. Hannula, H. Sorvoja, E. Alasaarela and R. Myllyla, “Measurement of respiratory rate with high-resolution accelerometer and EMFit pressure sensor,” *in Proc. IEEE Sensors Applicat. Symp.*, 2006, pp. 192-195, Houston, TX, USA.

[10] A. Loblaw, J. Nielsen, M. Okoniewski and M. A. Lakhani, “Remote respiratory sensing with an infrared camera using the Kinect (TM) infrared projector,” *in Proc. of Int. Conf. on Image Process., Comput. Vision, & Pattern Recognition* (*IPCV*), 2013, pp. 1-7, Las Vegas, NV, USA.

[11] K. S. Tan, R. Saatchi, H. Elphick and D. Burke, “Real-time vision based respiration monitoring system,” *in Proc. 7th Int. Symp. Commun. Syst., Networks & Digital Signal Process.* (*CSNDSP 2010*), 2010, pp. 770-774, Newcastle upon Tyne, United Kingdom.

[12] J. Shotton, R. Girshick, A. Fitzgibbon, T. Sharp, M. Cook, M. Finocchio, R. Moore, P. Kohli, A. Criminisi, A. Kipman and A. Blake, “Efficient human pose estimation from single depth images,” *IEEE Trans. Pattern Anal. Mach. Intell.*, vol. 35, no. 12, pp. 2821-2840, Dec. 2013.

[13] L. Xia, C. C. Chen and J. K. Aggarwal, "Human detection using depth information by Kinect," *in Proc. Comput. Vision and Pattern Recognition Workshops*, 2011, pp. 15-22, Colorado Springs, CO.

[14] A. R. Fekr, K. Radecka and Z. Zilic, “Design and evaluation of an intelligent remote tidal volume variability monitoring System in e-Health Applications,” *IEEE J. biomed. Informat.*, vol. 19, no. 5, pp. 1532-1548, Sep. 2015.

[15] G. F. Lewis, R. G. Gatto and S. W. Porges, “A novel method for extracting respiration rate and relative tidal volume from infrared thermography,” *Psychophysiology*, vol. 48, no. 7, pp. 877-887, Jul. 2011.

[16] J. Liu, Y. Wang, Y. Chen, J. Yang, X. Chen and J. Cheng, “Tracking vital signs during sleep leveraging off-the-shelf WiFi,” *in Proc. 16th ACM Int. Symp. Mobile Ad Hoc Networking & Comput.*, 2015, pp. 267-276, Hangzhou, China.

[17] X. Liu, J. Cao, S. Tang, J. Wen and P. Guo, “Contactless respiration monitoring via off-the-shelf WiFi device,” *IEEE Trans. Mobile Comput.*, vol. 15, no. 10, pp. 2466-2479, Oct. 2016.

[18] Y. Ma, G. Zhou, and S. Wang, “WiFi sensing with channel state information: A survey,” *ACM Computing Surveys*, vol. 52, no. 3, Article 46, pp. 1-36, Jun. 2019.

[19] D. Tse, and P. Viswanath, “Fundamentals of wireless communication,” *Cambridge university press*. 2005.

[20] D. Halperin, W. Hu, A. Sheth and D. Wetherall, “Tool release: gathering 802.11n traces with channel state information,” *Comput. Commun. Review*, vol. 41, no. 1, pp. 53, Jan. 2011.

[21] IEEE Std. 802.11n-2009, IEEE Standard for Information technology-- Local and metropolitan area networks-- Specific requirements-- Part 11: Wireless LAN Medium Access Control (MAC) and Physical Layer (PHY) Specifications Amendment 5: Enhancements for Higher Throughput, Oct. 2009.

[22] N. Patwari, J. Wilson, S. Ananthanarayanan, S. K. Kasera and D. R. Westenskow, “Monitoring breathing via signal strength in wireless networks,” *IEEE Trans. Mobile Comput.*, vol. 13, no. 8, pp. 1774-1786, Aug. 2014.

[23] N. Patwari, L. Brewer, Q. Tate, O. Kaltiokallio and M. Bocca, “Breathfinding: A wireless network that monitors and locates breathing in a home,” *IEEE J. Sel. Topics Signal Process.*, vol. 8, no. 1, pp. 30-42, Feb. 2014.

[24] H. Abdelnasser, K. A. Harras and M. Youssef, “UbiBreathe: A ubiquitous non-invasive WiFi-based breathing estimator,” *in Proc. of the 15th ACM Int. Symp. Mobile Ad Hoc Networking and Comput.*, 2015, pp. 277-286, Hangzhou, China.

[25] O. Kaltiokallio, H. Yiğitler, R. Jäntti and N. Patwari, “Non-invasive respiration rate monitoring using a single COTS TX-RX pair,” *in Proc. 13th Int. Symp. Inf. Process. Sens. Networks.*, 2014, pp. 59-69, Berlin, Germany.

[26] A. De Groote, M. Wantier, G. Chéron, M. Estenne and M. Paiva, “Chest wall motion during tidal breathing,” *J. Appl. Physiol.*, vol. 83, no. 5, pp. 1531-1537, Nov. 1997.

[27] X. Liu, J. Cao, S. Tang, and J. Wen, “Wi-Sleep: Contactless sleep monitoring via WiFi signals,” IEEE RTSS 2014, pp. 346-355

[28] F. Adib, H. Mao, Z. Kabelac, D. Katabi and R. C. Miller, “Smart homes that monitor breathing and heart rate,” *in Proc. 33rd Annu. ACM Conf. Human Factors Comput. Syst.*, 2015, pp. 837-846, Seoul, Republic of Korea.

[29] P. Nguyen, X. Zhang, A. Halbower, and T. Vu, "Continuous and Fine-grained Breathing Volume Monitoring from Afar Using Wireless Signals," IEEE INFOCOM 2016

[30] H. Wang, D. Zhang, J. Ma, Y. Wang, Y. Wang, D. Wu, T. Gu, and B. Xie, “Human respiration detection with commodity wifi devices: do user location and body orientation matter?,” ACM UbiComp 2016: 25-36.

[31] D. C. Montgomery, “Introduction to statistical quality control,” Wiley, 5th edition, 2005.

[32] METI, “HPS user guide”, Sarasota, FL: Medical Education Technologies, Inc., 2009, pp. 3.17 (83). [Online]. Available: http://caehealthcare.com//images/uploads/documents/HPS_User_Guide_v5.pdf

[33] D. Zhang, H. Wang, and D. Wu, “Toward Centimeter-Scale Human Activity Sensing with Wi-Fi Signals,” IEEE Computer 50(1): 48-57 (2017)

This article has been accepted for publication in a future issue of this journal, but has not been fully edited. Content may change prior to final publication. Citation information: DOI 10.1109/JSEN.2020.3023178, IEEE Sensors Journal

[34] R. Wilson, "Propagation losses through common building materials 2.4 GHz vs 5 GHz," Magis networks Inc, Technical report, 2009.

[35] P. E. Watson, I. D. Watson and R. D. Batt, "Total body water volumes for adult males and females estimated from simple anthropometric measurements," *Amer. J. clinical nutrition*, vol. 33, no. 1, 1980, pp. 27-39, Jan. 1980.

[36] J-P. Eckmann, S. O. Kamphorst, and D. R. "Recurrence plots of dynamical systems." EPL (Europhysics Letters) vol. 4, no. 9, pp. 973, 1987

[37] W. S. Lim, S. M. Carty, J. T. Macfarlane, R. E. Anthony, J. Christian, K. S. Dakin and P. M. Dennis, "Respiratory rate measurement in adults--how reliable is it?," *Respiratory Medicine*, vol. 96, no. 1, pp. 31-3, Jan. 2002.

[38] L. G. Nielsen, L. Folkestad, J. B. Brodersen and M. Brabrand, "Inter-observer agreement in measuring respiratory rate," PloS One, Jun. 2015, 10(6):e0129493.
doi: 10.1371/journal.pone.0129493. eCollection.